Sensors and Materials, Vol. 36, No. 8 (2024) 3609–3624
MYU Tokyo

S & M 3753

Sensor-data-based Photovoltaic Power Prediction Using Support Vector Machine Optimized by Improved Dragonfly Algorithm

Jincai Niu,[1,2] Yu Tang,[1,2] and Hsiung-Cheng Lin[3*]

[1]State Key Laboratory of Reliability and Intelligence of Electrical Equipment, Hebei University of Technology, Tianjin 300401, China
[2]Key Laboratory of Electromagnetic Field and Electrical Apparatus Reliability of Hebei Province, Hebei University of Technology, Tianjin 300130, China
[3]Department of Electronic Engineering, National Chin-Yi University of Technology, Taichung 41170, Taiwan

(Received November 26, 2023; accepted April 15, 2024)

Keywords: new energy, photovoltaic system, power prediction, intelligent algorithm, support vector machine, economic dispatch

A large-scale integration of photovoltaic (PV) systems can degrade the stability of the power grid. Therefore, it is important to accurately predict the short-term output power generated from PV systems to achieve better grid power distribution and allocation. For this reason, a short-term PV power prediction model that uses the data collected from temperature sensors, irradiance sensors, and other relevant sensors was proposed, in which an improved dragonfly algorithm (IDA) was applied to optimize the support vector machine (SVM). First, the output power curves of PV systems under sunny, cloudy, and rainy conditions were analyzed to determine the input variables of the prediction model, which included temperature, relative humidity, and solar radiation intensity. Second, the original dragonfly algorithm in the optimization process was improved, and then, this IDA was utilized to optimize the parameters of SVM, enhancing the predictive capability of the model. Finally, the IDA-optimized SVM (IDA-SVM) model was applied to predict the PV output power. Test performance results demonstrated that the average absolute percentage errors of IDA-SVM were 2.42, 5.96, and 7.44% for sunny, cloudy, and rainy days, respectively, outperforming other comparative models. The performance results showed that the proposed model can not only improve the stability of PV integration, but also effectively increase the penetration rate of PV energy and enhance the reliability of power system operation.

1. Introduction

Renewable energy systems are increasingly being applied worldwide, with solar energy being considered a major renewable energy resource.[1,2] However, the photovoltaic (PV) output power is strongly related to weather conditions; thus, it is very uncertain and nonstationary.[3,4] To solve this problem, it is crucial to accurately predict the PV power generation.[5] Sharadga *et al.*[6] introduced several time series prediction methods, including statistical and artificial intelligence methods for PV power prediction. Alsharif *et al.*[7] proposed a seasonal autoregressive integrated

*Corresponding author: e-mail: hclin@ncut.edu.tw
https://doi.org/10.18494/SAM4809

ISSN 0914-4935
https://myukk.org/

moving average (SARIMA) model for predicting daily and monthly solar radiations in Seoul, Korea. The results showed that the model exhibited a good fit. However, it was only better when applied in ultrashort-term prediction. To improve the performance of the time series method in longer prediction periods, Ren *et al.*[8] combined SARIMA and support vector machine (SVM) to build a new hybrid prediction model that outperformed SARIMA and SVM alone.

Recently, machine learning algorithms have been widely used owing to their simplicity of operation and ability to deal with nonlinear problems.[9] Common machine-learning-based forecasting models mainly include the artificial neural network (ANN), grey theory, and SVM. Among them, grey theory requires that the initial data sequence satisfies the law of exponential growth, and a very fast sequence change will also lead to a decline in fitting ability. Therefore, grey theory cannot fully adapt to the PV output affected by changeable weather, so it is not practical in PV power prediction.[6] Neural network models in specific cases can attain a high prediction accuracy, but traditional ANNs are affected by their own weights and parameter selection and thus likely produce large errors. Moreover, the model used for a neural network structure containing multiple hidden layers requires a massive amount of training data, increasing its complexity and training time and reducing its convergence speed.[7] Bouzerdoum *et al.*[10] presented a hybrid framework of a prediction model and uncertainty evaluation based on Gaussian process regression and the Kalman filter. The results showed that their prediction accuracy was higher than those of some existing methods. Theocharides *et al.*[11] proposed a PV power generation forecasting model optimized by differential evolution and particle swarm optimization (PSO). Their results demonstrated that the approach is more efficient and accurate than a traditional method. Faris *et al.*[12] proposed a hybrid prediction model based on the radial basis neural network and gray prediction algorithm for PV output power prediction for different seasons. The results showed that it has a higher prediction ability than the original prediction models. In addition, the learning machine model such as SVM can converge quickly. However, the fitting ability for time-series data is not high, and the model parameter search lacks robustness.[13] Moreover, the computational performance of SVM is highly dependent on the model kernel function.[14] Therefore, there is a need to continuously improve or explore new algorithms to realize more accurate predictions.

Meng *et al.*[15] combined wavelet transform, PSO, and SVM for a short-term PV power forecast. In the proposed model, wavelets were used to process the training data and PSO was used to optimize the parameters of SVM. Seyedmahmoudian *et al.*[16] divided the weather data into specific categories by means of fuzzy inference, and then, used the SVM model for each category of weather for prediction. The prediction results proved that SVM has a good effect on different types of weather. Jaziri *et al.*[17] adopted least-squares SVM and analyzed the system efficiency of solar air heaters. The performance of the SVM model was improved, but the prediction results remained poor owing to its own shortcomings.

The structure of the remaining sections is as follows. In Sect. 2, we introduce the principle of SVM and propose the improved dragonfly algorithm (IDA). In Sect. 3, we analyze the factors affecting PV power and determine the inputs and outputs of the PV power prediction model. In Sect. 4, we test and validate the IDA and IDA-optimized SVM (IDA-SVM) model. In Sect. 5, we present the conclusions of this study.

2. PV Output Power Prediction Model Based on Sensor Data

2.1 SVM model

We first outline the SVM model used for optimization in this study. SVM can map low-dimensional samples into a higher dimensional space R_n to better solve classification and nonlinear regression problems.

The functional relationship of SVM is expressed as

$$y(x) = \omega^T x + b, \tag{1}$$

where $y(x)$ is the predicted value corresponding to x, b is the bias term, and ω is the weight coefficient.

SVM is used to minimize the error between $y(x)$ and the actual value. To strengthen the SVM generalization ability during the model process, the objective function and constraint conditions are respectively defined as

$$\max\left(\frac{1}{\|\omega\|} - C\sum_{i=1}^{n}\xi_i\right), \tag{2}$$

$$\begin{cases} y_i\left(\omega^T \cdot x_i - b\right) \geq 1 - \xi_i \\ \xi_i \geq 0 \quad (i = 1, 2, \ldots n) \end{cases}, \tag{3}$$

where ξ_i is the relaxation factor; C is the penalty factor, which constrains ξ_i; x_i and y_i are the inputs and outputs of the model training samples, respectively; $i \in [1, 2, ..., n]$, where n is the number of samples.

We consider the effects of factors such as temperature and radiance on PV power. Therefore, a kernel function is added to the SVM regression equation, as follows:

$$y(x) = \sum_{i=1}^{n}\alpha_i y_i K(x, x_i) + b, \tag{4}$$

where α_i is the Lagrange multiplier introduced to solve eq. (2); $K(x, x_i)$ is the kernel function, $K(x, x_i) = \varphi(x) \cdot \varphi(x_i)$; and $\varphi(x)$ is the mapping function of data from low-dimensional space to high-dimensional space.

In this study, the radial basis function (RBF) is selected as the kernel function. Accordingly, it is expressed as

$$K\left(x,x_i\right)=\exp\left(-\frac{\left\|x-x_i\right\|}{\delta^2}\right), \tag{5}$$

where $\delta > 0$ is the bandwidth of RBF.

In SVM, the kernel function parameter δ and the penalty factor C are randomly selected, which can affect the predictive performance of SVM. In this study, we optimize the selection of values (C, δ) in SVM by using the dragonfly algorithm (DA). DA is used to determine the performance parameter combination of SVM to maximize the predictive performance.

2.2 IDA

DA is a swarm intelligence algorithm that simulates the swarm behavior of dragonflies in nature.[13] In this study, adaptive factors and differential variation strategies are introduced into DA to improve its performance. IDA is as follows.

2.2.1 Adaptive factor

The adaptive factor c_t is added to DA to enhance its search capability and expressed as

$$c_t=\frac{1}{1+e^{-n}}, \tag{6}$$

where n is the relative rate of change, which is defined as

$$n=\frac{\left|F_i-F_{best}\right|}{F_{best}}. \tag{7}$$

Here, F_{best} is the best fitness value in the current iteration and F_i is the objective function value of the ith dragonfly.

Accordingly, the updating of dragonfly positions in static group behavior is expressed as

$$Y_{t+1}=c_tY_t+\Delta Y_{t+1}. \tag{8}$$

The equation for updating the position of a dragonfly in dynamic group behavior is expressed as

$$Y_{t+1}=c_tY_t+Le'vy\left(dim\right)\times Y_t, \tag{9}$$

where t is the number of iterations; Y_t and Y_{t+1} are the positions of the dragonfly at the tth and (t + 1)th iterations, respectively; and dim is the dimension of the position vector. The mathematical expression for $Le'vy$ flight is expressed as

$$Le'vy(x) = 0.01 \times \frac{r_1 \times \sigma}{|r_2|^{\frac{1}{\beta}}}, \tag{10}$$

where r_1 and r_2 are random numbers that belong to [0, 1] and β is a constant with a value of 1.5. The expression of σ is shown as

$$\sigma = \left\{ \frac{T(1+\beta) \times \sin\left(\frac{\pi\beta}{2}\right)}{T\left(\frac{1+\beta}{2}\right) \times \beta \times 2^{\left(\frac{\beta-1}{2}\right)}} \right\}^{\frac{1}{\beta}}, \tag{11}$$

where $T(x) = (x - 1)!$.

2.2.2 Differential variation strategy

The differential variation strategy is introduced to DA; it includes three operations, namely, the generation of variant individuals, crossover operation, and merit selection operation.

First, three different populations of individuals, Y_k, Y_1, and Y_2, are randomly selected, and the position of Y_k is updated.

$$Y_k = Y_{best} + \mu \cdot (Y_1 - Y_2) \tag{12}$$

Y_{best} is the position of the optimal individual and μ is the differential variance factor, which is expressed as

$$\mu = \mu_l + (\mu_u - \mu_l) \times \frac{F_k - F_{best}}{F_{worst} - F_{best}}, \tag{13}$$

where μ_u and μ_l are the maximum (0.9) and minimum (0.1) values of μ, and F_{best} and F_{worst} are the best and worst fitness values, respectively.

Next, the crossover operation is performed on mutated populations with a crossover factor of *pCR*, which is calculated as

$$pCR = \frac{1}{2} \times (1 + rand(0,1)), \tag{14}$$

where *pCR* is a random number between 0 and 1. In the crossover operation, a number *r* between 0 and 1 is randomly generated. If *r* is greater than *pCR*, the individual before the crossover is replaced by the individual after the crossover, and if vice versa, the position of the individual remains unchanged. After the crossover operation, the fitness value of the new population is calculated to finally determine the best dragonfly position.

3. Analysis of Factors Affecting PV Power

In this study, the PV output power under sunny, cloudy, and rainy days was selected to test the proposed model on the basis of the historical data of the DKASC PV plant in Australia in 2016. The PV output power curves under three different weather conditions between 8:00 and 17:55 recorded every 5 min are plotted in Fig. 1.

From Fig. 1, it can be seen that the PV output power curve on sunny days is smooth and reaches the maximum at 12:00–13:00. On rainy days, the overall solar radiation intensity is lower than other days such that the PV output power is lower. Under cloudy weather, the light intensity shows a similar trend to that on a sunny day, but the PV output power is more volatile. In reality, many external environmental factors also affect PV power, including temperature, solar radiation intensity, and the relative humidity of air. Figure 2 shows the plots of PV output power with temperature, solar radiation intensity, and relative humidity.

Figure 2(a) indicates a low correlation between temperature and output power. Figure 2(b) indicates a negative correlation between PV power and relative humidity. Figure 2(c) indicates a high correlation between solar radiation intensity and output power.

4. Test and Outcome Analysis

4.1 Test functions

Five classical functions in Table 1 were chosen to verify the convergence ability of IDA, where F_1 and F_2 are single-peaked functions, and F_3, F_4, and F_5 are multipeaked functions. The PSO, optimal foraging algorithm (OFA), gray wolf optimization (GWO), DA, and IDA were selected to test the functions. All algorithms were carried out using MATLAB 2021a with a maximum of 30 iterations. c_1 and c_2 of PSO were set to 0.72. The constant factor β in DA and IDA was set to 1.5. The cross factor in IDA was set to 0.6. The mean and standard deviation of

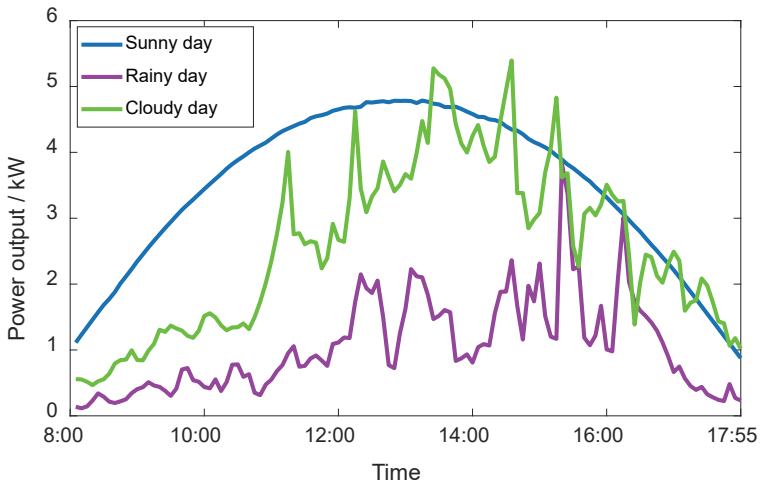

Fig. 1. (Color online) PV output power curves under different weather situations.

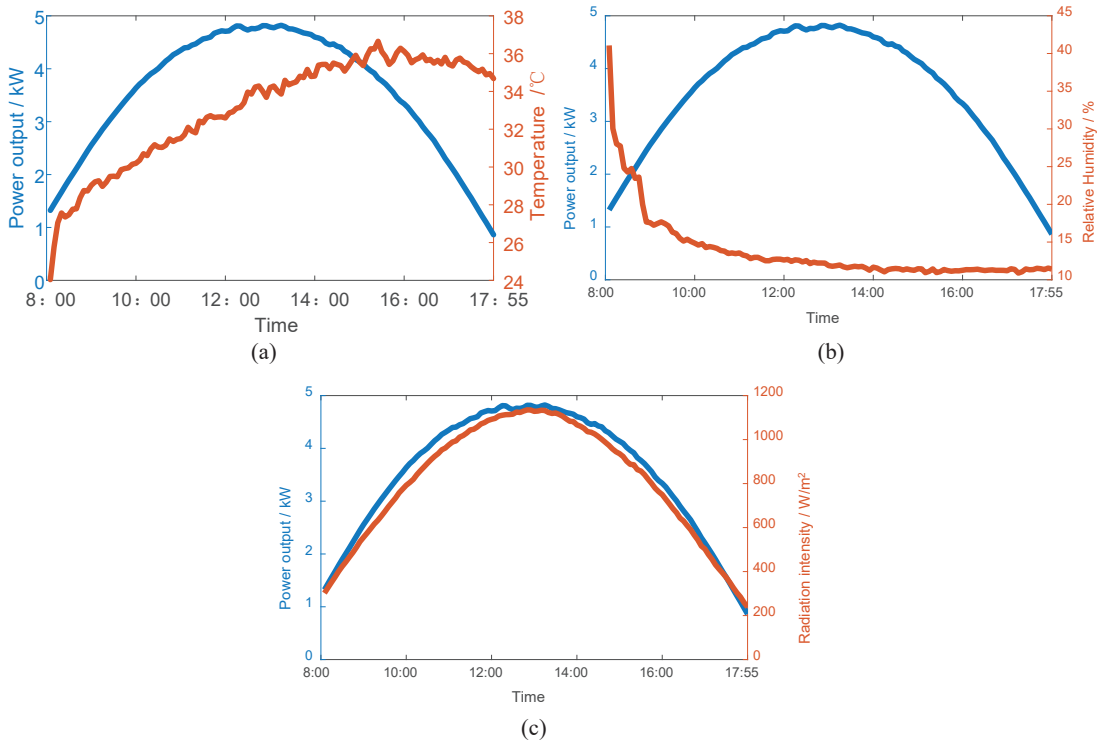

Fig. 2. (Color online) Correlation curves between three meteorological factors and PV power. (a) Correlation between temperature and PV power. (b) Correlation between relative humidity and PV power. (c) Correlation between radiation intensity and PV power.

Table 1
Test functions.

	Range	Optimum value
$F_1(x)=\sum_{i=1}^{n}x_i^2$	[−100, 100]	0
$F_2(x)=\sum_{i=1}^{n}\lvert x_i\rvert+\prod_{i=1}^{n}\lvert x_i\rvert$	[−10, 10]	0
$F_3(x)=\sum_{i=1}^{n}\left[x_i^2-10\cos(2\pi x_i)+10\right]$	[−5.12, 5.12]	0
$F_4(x)=-20\exp\left(-0.2\sqrt{\frac{1}{n}\sum_{i=1}^{n}x_i^2}\right)-\exp\left[\frac{1}{n}\sum_{i=1}^{n}\cos(2\pi x_i)\right]+20+e$	[−32, 32]	0
$F_5(x)=\frac{1}{4000}\sum_{i=1}^{n}x_i^2-\prod_{i=1}^{n}\cos\left(\frac{x_i}{\sqrt{i}}\right)+1$	[−600, 600]	0

the results of 30 tests were used as performance indicators. The statistical results are shown in Table 2.

The results reveal that the optimal solution provided by IDA is better than those given by the other algorithms and achieves the highest accuracy. Simultaneously, it has the lowest standard deviation and average. In particular, the standard deviation of IDA in F_3 and F_5 reaches 0, and in F_1, F_2, and F_4, the standard deviation is the smallest. It is proved that the proposed method has good optimization stability.

Table 2
Test results of PSO, OFA, GWO, DA, and IDA.

F	Statistical values	PSO	OFA	GWO	DA	IDA
F_1	Average value	0.24	5.20×10^{3}	$9.27\text{E} \times 10^{-9}$	1.44×10^{3}	1.27×10^{-35}
	Standard deviation	0.16	3.86×10^{3}	$6.40\text{E} \times 10^{-9}$	405.70	3.73×10^{-35}
F_2	Average value	1.44	1.05×10^{5}	5.52×10^{-6}	17.24	4.10×10^{-19}
	Standard deviation	0.54	1.02×10^{5}	2.82×10^{-6}	2.36	1.03×10^{-18}
F_3	Average value	95.06	268.13	11.22	164.26	0
	Standard deviation	29.30	180.60	7.06	19.26	0
F_4	Average value	1.26×10^{-4}	5.60	2.04×10^{-11}	5.74	4.68×10^{-15}
	Standard deviation	8.74×10^{-5}	3.22	1.91×10^{-11}	1.05	1.30×10^{-15}
F_5	Average value	6.51	50.06	$1.54\text{E} \times 10^{-2}$	14.23	0
	Standard deviation	2.91	40.20	2.11×10^{-2}	3.81	0

4.2 Implementation of IDA-SVM prediction model

The flowchart of the IDA-SVM prediction model is shown in Fig. 3.

(1) Obtain the PV prediction dataset based on sensor data, including radiation intensity, temperature, relative humidity, and PV output power.
(2) Normalize PV data and divide them into testing and training data.
(3) Set parameters: the max-iteration is 30, the population is 30, the dimension is 2, the range of the penalty factor C is [0.1, 1200], and the range of the function parameter δ is [0.01, 100]. Other parameters have default values.
(4) IDA starts iterative optimization using the training dataset, where the root mean square error (*RMSE*) is selected as the objective function for optimization.
(5) Judge whether IDA has reached optimal convergence. If yes, the optimal output is obtained as the individual position $d(d_1, d_2)$ at this time; if not, continue to proceed with optimization.
(6) The optimal individual position $d(d_1, d_2)$ corresponds to (C, δ) in SVM.
(7) IDA-SVM is used to predict the testing data to obtain the output.

4.3 Model evaluation

The data obtained on January 21 (sunny day), February 26 (cloudy day), and March 29 (rainy day) from the DKASC PV plant in Australia were used for testing the model. The data from a period of 10 days before the date of collection of the test data were used for the training process. *RMSE*, mean absolute percentage error (*MAPE*), mean absolute error (*MAE*), the maximum value of absolute error (AE_{max}), and the maximum value of relative error (RE_{max}) were chosen to evaluate the model performance. They are expressed as follows.

$$RMSE = \sqrt{\frac{1}{M}\sum_{i}^{M}\left(P_{pre} - P_{re}\right)^2} \times 100\% \tag{15}$$

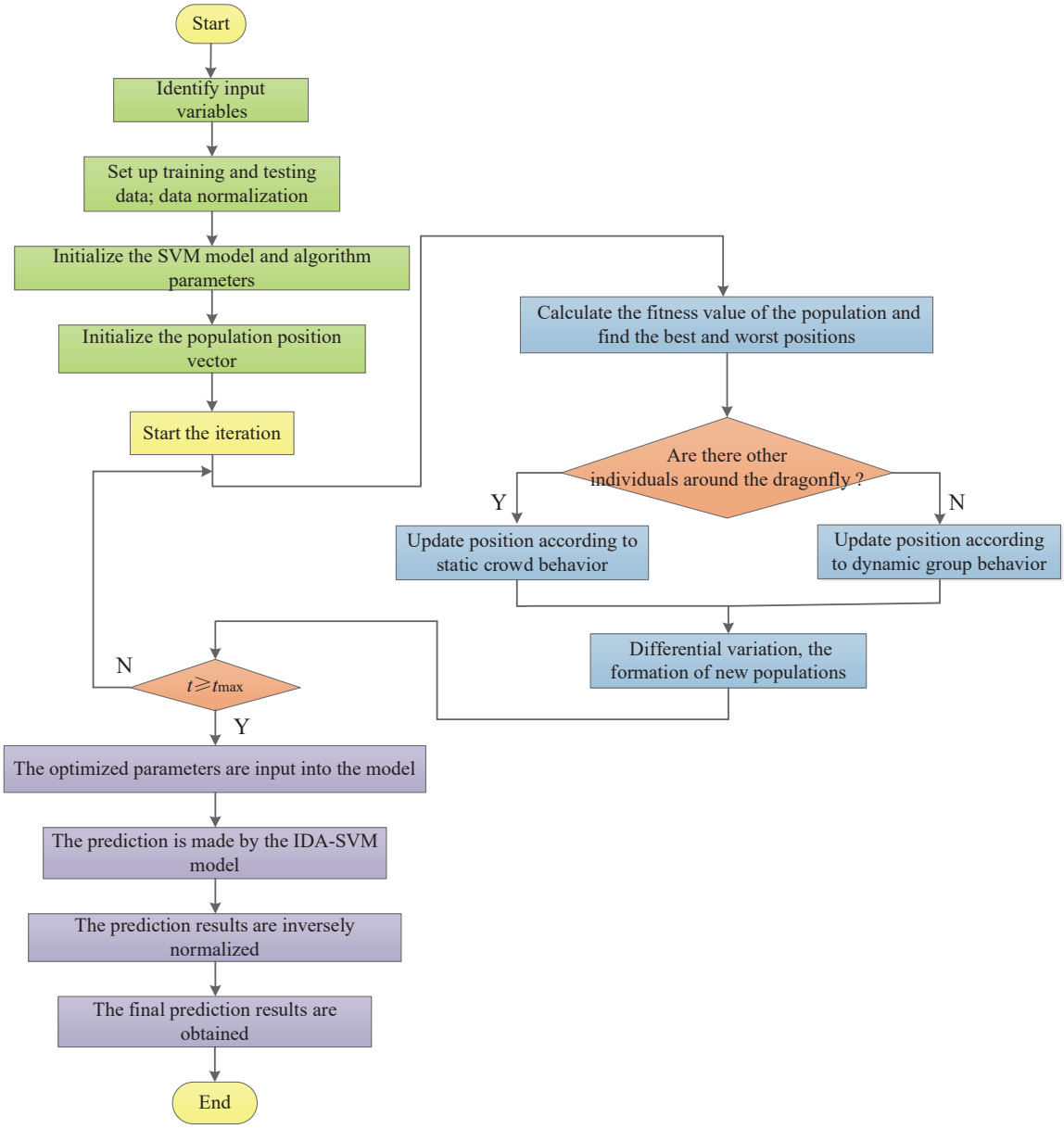

Fig. 3. (Color online) Flowchart of IDA-SVM prediction model.

$$MAPE = \frac{1}{M}\sum_{i}^{M}\left|\frac{P_{pre} - p_{re}}{P_{pre}}\right| \times 100\% \tag{16}$$

$$MAE = \frac{1}{M}\sum_{i}^{M}\left|P_{pre} - p_{re}\right| \times 100\% \tag{17}$$

$$AE_{max} = \max\left\{\left|P_{prei} - p_{rei}\right|\right\} \quad i = 1,2,\ldots,M \tag{18}$$

$$RE_{max} = \max\left\{\left|\frac{P_{prei} - p_{rei}}{p_{rei}}\right| \times 100\%\right\} \quad i = 1,2,\ldots,M \tag{19}$$

Here, M is the total number of samples, P_{pre} is the predicted PV output power, and P_{re} is the true value. In addition, to evaluate the computational complexity of the model, the time t (s) was selected in this study.

4.3.1 Case 1: On sunny days

Dragonfly Algorithm optimized Support Vector Machine (DA-SVM), Optimal Foraging Algorithm optimized Support Vector Machine (OFA-SVM), SVM, and backpropagation algorithm (BP) models were used for comparison, where BP is a multilayer feedforward neural network with error backpropagation and signal forward propagation. On sunny days, the historical PV power data obtained from January 10 to 20 were selected for training the model, and the data from January 21 were used for prediction. The prediction results are shown in Fig. 4.

From Fig. 4, the PV output power curves from all algorithms indicate a smooth rising trend from 8:00 to 13:00 and a smooth falling trend from 13:00 to 15:55. Among them, the prediction curve of IDA-SVM is most consistent with the actual curve. In the time period of 8:00–14:00, the curves of OFA-SVM, BP, and SVM clearly deviated from the actual output, but only SVM

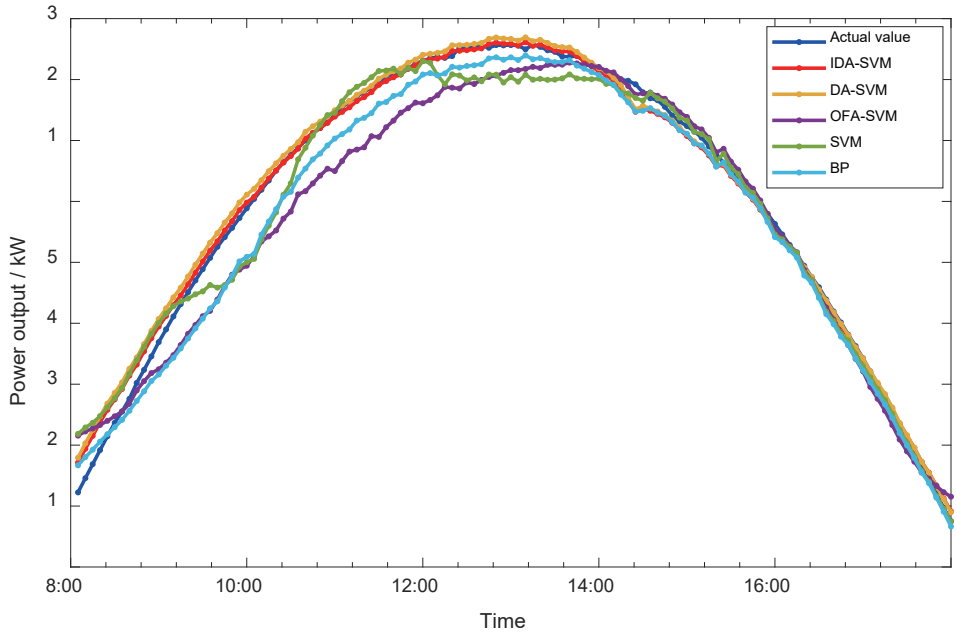

Fig. 4. (Color online) Prediction results of five algorithms on sunny days.

has a significant fluctuation. After 14:00, all the models fit the actual PV output curve. In this study, absolute error (*AE*), relative error (*RE*), *MAE*, *MAPE*, and *RMSE* were selected to evaluate the effectiveness of prediction performance. Prediction errors based on the above evaluation tools are shown in Table 3, and *RE* curves are shown in Fig. 5.

As shown in Table 3, the *MAE* values of IDA-SVM decreased by 24.49, 72.52, 62.42, and 58.84% compared with those of DA-SVM, OFA-SVM, BP, and SVM, respectively. The *MAPE* values of IDA-SVM decreased by 0.65, 4.06, 2.27, and 2.8% compared with those of DA-SVM, OFA-SVM, BP, and SVM, respectively. The *RMSE* values of IDA-SVM decreased by 2.08, 32.47, 10.41, and 10.17% compared with those of DA-SVM, OFA-SVM, BP, and SVM, respectively. However, the IDA-SVM prediction required the longest computational time among all the algorithms.

In Fig. 5, the IDA-SVM model presents the smallest *RE* and the smoothest curve among the five models. DA-SVM is poorer than IDA-SVM and OFA-SVM. BP and SVM have large *RE*s in most periods of time. The *RE* of IDA-SVM decreases steadily from 8:00 to 10:00 and shows only a slight fluctuation close to 0 after 10:00. The trend of the DA-SVM curve is the same as that of the IDA-SVM curve, but *RE* is larger. Although the *RE*s of OFA-SVM, BP, and SVM decrease rapidly before 9:00, they show a significant fluctuation after 9:00.

Table 3
Prediction errors on sunny days.

Model	AE_{max}	*MAE*	RE_{max} (%)	*MAPE* (%)	*RMSE* (%)	*t* (s)
IDA-SVM	0.2440	0.0552	21.94	2.42	8.04	234.09
DA-SVM	0.2862	0.0731	25.57	3.07	10.12	71.52
OFA-SVM	0.4656	0.2009	41.86	6.48	40.51	35.68
BP	0.4513	0.1469	19.92	4.69	18.45	1.86
SVM	0.4920	0.1341	43.15	4.60	18.21	0.51

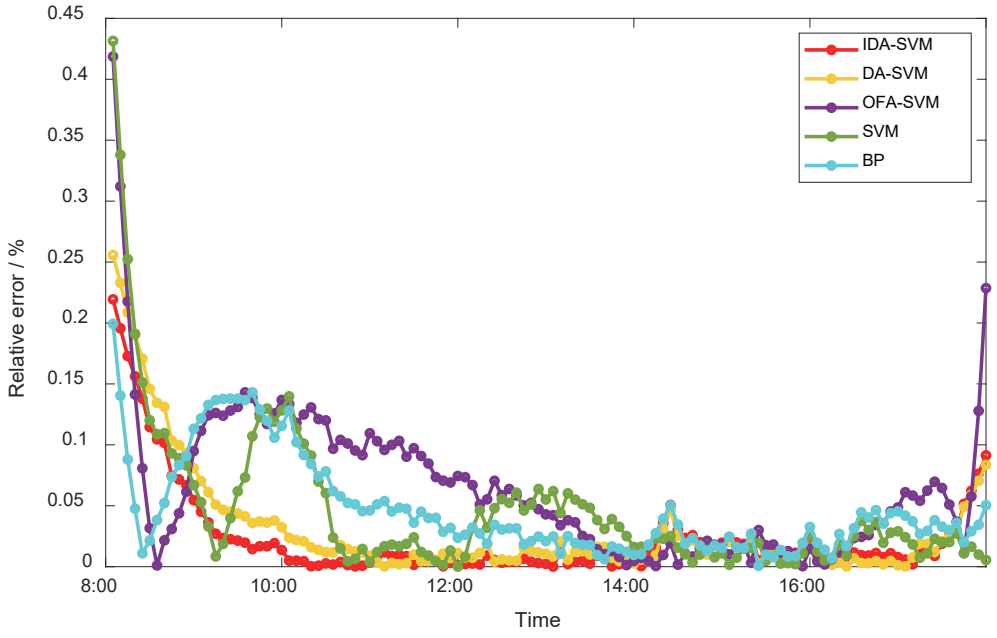

Fig. 5. (Color online) *RE* curves on sunny days.

4.3.2 Case 2: On cloudy days

On cloudy days, the historical PV output data from February 15 to 25 were selected for the training process, and the data from Feb. 26 were used for prediction. The prediction results on cloudy days are shown in Fig. 6.

Figure 6 shows that under cloudy weather, the light intensity changes rapidly. Compared with the other model curves, the IDA-SVM prediction model curve shows a better result, maintaining almost the same value as the actual curve in most of the time periods except around 14:00. The error values are shown in Table 4, and the *RE* curves are shown in Fig. 7.

As seen in Table 4, the *MAE* values of IDA-SVM decreased by 38.48, 32.37, 9.43, and 33.30% compared with those of DA-SVM, OFA-SVM, BP, and SVM, respectively. The *MAPE* values of IDA-SVM decreased by 7.45, 4.24, 0.82, and 5.86% compared with those of DA-SVM, OFA-SVM, BP, and SVM, respectively. The *RMSE* values of IDA-SVM decreased by 8.11, 15.51, 0.39, and 4.01% compared with those of DA-SVM, OFA-SVM, BP, and SVM, respectively. In the prediction results, the AE_{max} values of IDA-SVM and DA-SVM are slightly higher than those of

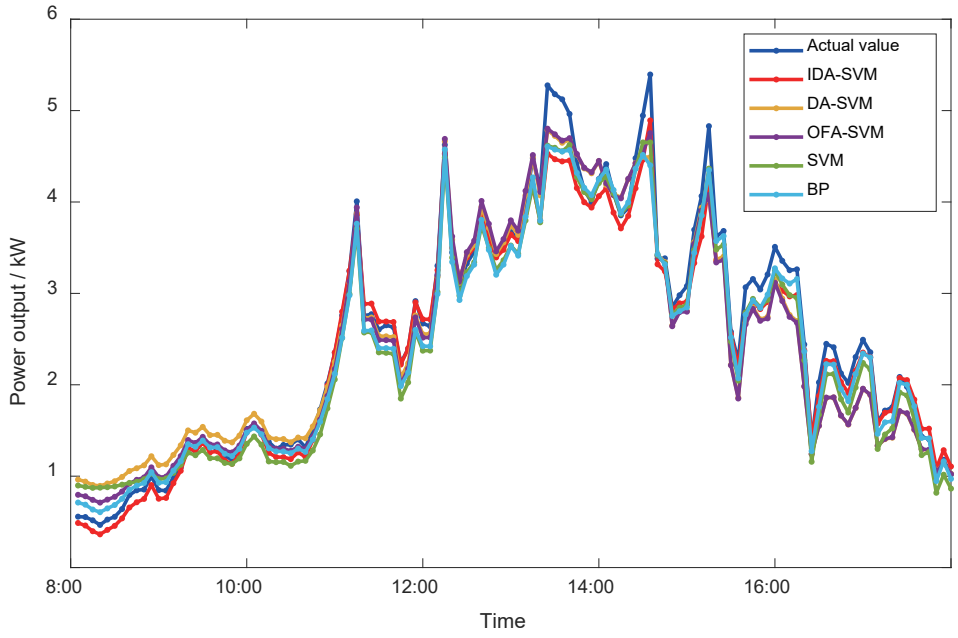

Fig. 6. (Color online) Prediction results of five models on cloudy days.

Table 4
Prediction errors of five models on cloudy days.

Model	AE_{max}	*MAE*	RE_{max} (%)	*MAPE* (%)	*RMSE* (%)	*t* (s)
IDA-SVM	0.7487	0.1402	23.12	5.96	20.68	258.07
DA-SVM	0.9050	0.2279	91.51	13.41	28.79	157.33
OFA-SVM	0.6415	0.2073	52.35	10.20	36.19	116.05
BP	0.6692	0.1548	27.68	6.78	21.07	1.24
SVM	0.6599	0.2102	87.36	11.82	24.69	0.44

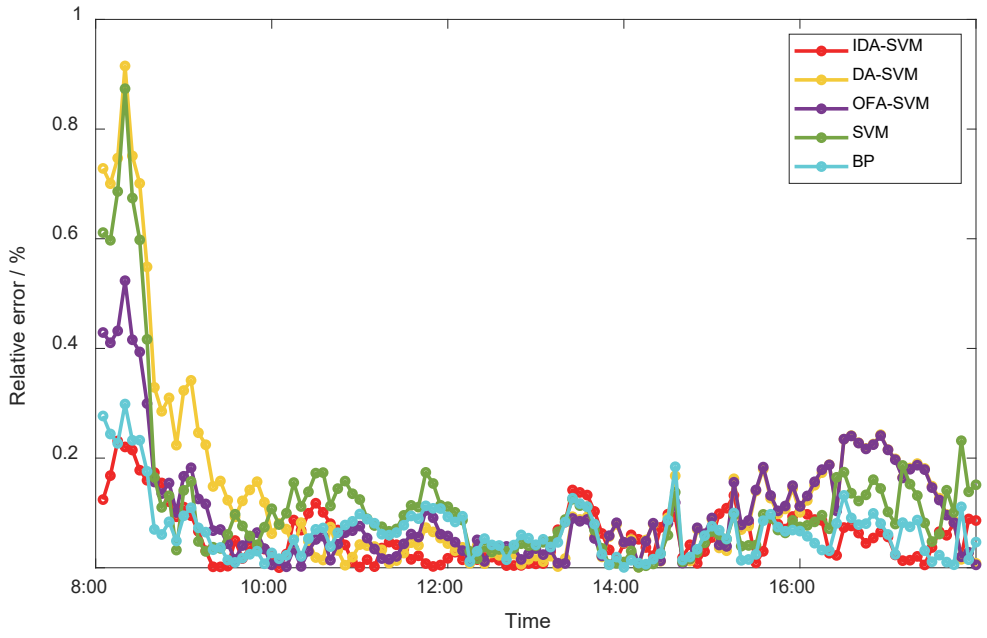

Fig. 7. (Color online) *RE* curves of five models on cloudy days.

the other models. Nevertheless, in general, IDA-SVM has the smallest error and confirms a higher prediction performance.

Figure 7 shows that the error curves for all five models show similar trends. *RE* increased initially and then decreased abruptly from 8:00 to 9:00. After 10:00, all *RE*s reached a lower level relative to 0. Among them, the IDA-SVM model has less fluctuation. On the other hand, the *RE* of the DA-SVM prediction reached a high level before 10:00 and subsequently decreased. However, the *RE*s of OFA-SVM, BP, and SVM models remained high at most times.

4.3.3 Case 3: On rainy days

On rainy days, the historical PV output data obtained from March 19 to 28 were selected for training, and the data from March 29 were selected for prediction. The prediction results obtained using five models on rainy days are shown in Fig. 8. It is found that the IDA-SVM model prediction curve is closest to the actual curve, and the OFA-SVM model has the worst prediction effect owing to a significant deviation at most times.

In Table 5, the *MAE* values of IDA-SVM decreased by 0.0113, 0.0456, 0.049, and 0.0509 compared with those of DA-SVM, OFA-SVM, BP, and SVM, respectively. The *MAPE* values of IDA-SVM decreased by 1.37, 7.68, 8.06, and 9.95% compared with those of DA-SVM, OFA-SVM, BP, and SVM, respectively. The *RMSE* values of IDA-SVM decreased by 0.97, 18.28, 5.19, and 5.6% compared with those of DA-SVM, OFA-SVM, BP, and SVM, respectively. IDA-SVM yields the best results for all five indicators, which is consistent with the results shown in Fig. 9.

In Fig. 9, the *RE* of IDA-SVM is less than those of the other four models at most times. At the beginning, the *RE*s of OFA-SVM and SVM were large, and those of DA-SVM and IDA-SVM

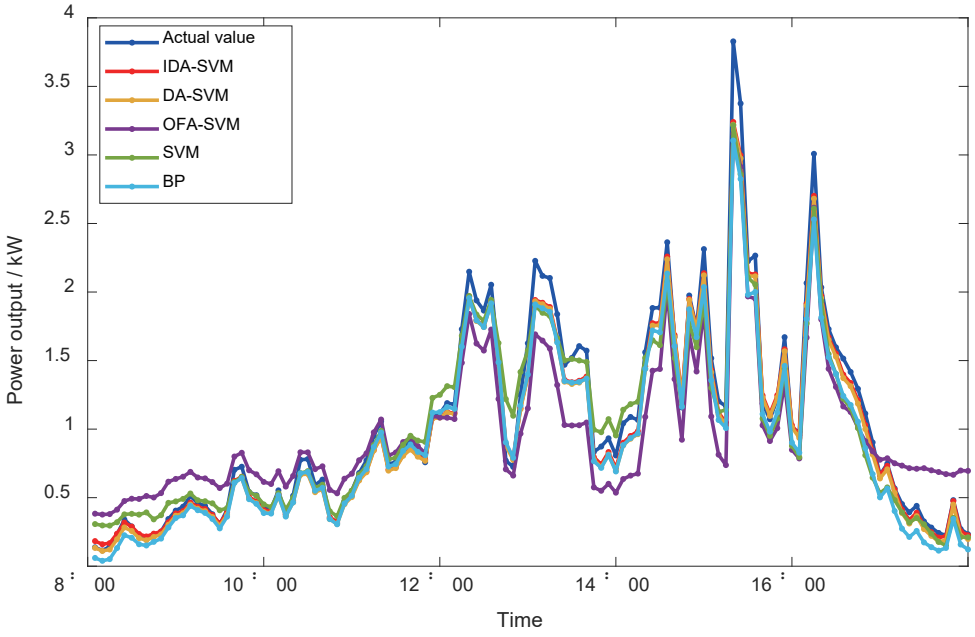

Fig. 8. (Color online) Prediction results of five models on rainy days.

Table 5
Prediction errors of five models on rainy days.

Model	AE_{max}	MAE	RE_{max} (%)	$MAPE$ (%)	$RMSE$ (%)	t (s)
IDA-SVM	0.5877	0.0772	39.40	7.44	11.32	227.46
DA-SVM	0.6080	0.0885	45.74	8.81	12.29	90.77
OFA-SVM	0.7452	0.1228	138.82	15.12	29.60	50.04
BP	0.7231	0.1262	65.74	15.50	16.51	1.30
SVM	0.6113	0.1281	158.92	17.39	16.92	0.53

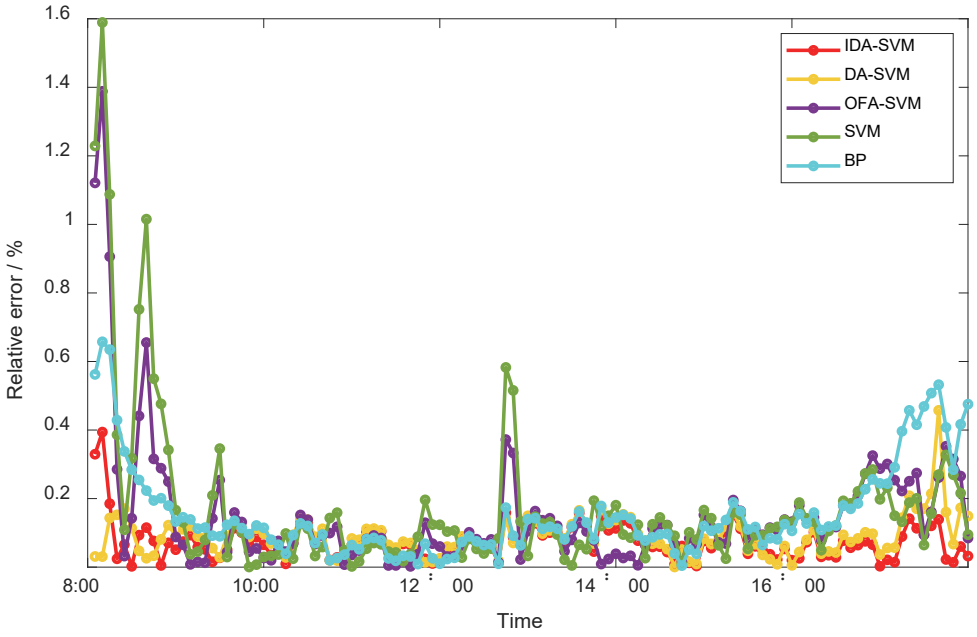

Fig. 9. (Color online) *RE* curves of five models on rainy days.

were small. On the other hand, OFA-SVM and SVM had sharp fluctuations at 8:00–10:00 and 13:00, indicating poor performance. Although the *RE* of IDA-SVM initially was higher than that of DA-SVM, it was almost close to 0 at most other times.

5. Conclusions

For the integrated energy system or microgrid with PV power generation, the formulation of its dispatching strategy based on accurate power prediction needs to be addressed. In this study, the short-term PV power prediction method based on the IDA-SVM model achieved a higher prediction ability under different weather conditions than DA-SVM, OFA-SVM, SVM, and BP approaches. The test results verify that the IDA-SVM model can effectively improve the accuracy in short-term PV power prediction and thus enable the acceptance of PV energy in the power grid. However, the running time of the IDA-SVM model is slightly longer than those of the other existing models in obtaining prediction results with higher precision. Nevertheless, in practice, with the effect of considerably improving the prediction accuracy, the running time using the IDA-SVM model is satisfactory for prediction for the next 1–2 days. It can be concluded that the IDA-SVM model provides the best solution for PV output power prediction regardless of weather conditions.

The proposed short-term PV power prediction model can not only improve the operational efficiency of PV power generation systems, but also provide a crucial guideline for the development of intelligent energy management systems, further promoting the application and popularization of clean energy. The use of samples of these three weather conditions enables the model to gain a deeper understanding of the trends in PV power generation under different meteorological backgrounds. This training method can allow the model to more comprehensively adapt to diverse weather conditions, thereby improving its prediction accuracy under unknown weather conditions.

References

1. L.-L. Li, Z.-F. Liu, M.-L. Tseng, S.-J. Zheng, and M. K. Lim: Appl. Soft Comput. **108** (2021) 107504. https://doi.org/10.1016/j.asoc.2021.107504
2 Y. Feng, W. Hao, H. Li, N. Cui, D. Gong, and L. Gao: Renewable Sustainable Energy Rev. **118** (2020) 109393. https://doi.org/10.1016/j.rser.2019.109393
3 S. Choudhury, P. Bhowmik, and P. K. Rout: Sustainable Cities Soc. **37** (2017) 550. https://doi.org/10.1016/j.scs.2017.11.013
4 N. Dong, J.-F. Chang, A.-G. Wu, and Z.-K. Gao: Int. J. Electr. Power Energy Syst. **114** (2020) 105411. https://doi.org/10.1016/j.ijepes.2019.105411
5 L. Wen, K. Zhou, S. Yang, and X. Lu: Energy **171** (2019) 1053. https://doi.org/10.1016/j.energy.2019.01.075
6 H. Sharadga, S. Hajimirza, and R. S. Balog: Renewable Energy **150** (2020) 797. https://doi.org/10.1016/j.renene.2019.12.131
7 M. H. Alsharif, M. K. Younes, and J. Kim: Symmetry **11** (2019) 240. https://doi.org/10.3390/sym11020240
8 L. Ren, F. Kong, X. Wang, Y. Song, X. Li, F. Zhang, N. Sun, H. An, Z. Jiang, and J. Wang: Nano Energy **98** (2022) 107248. https://doi.org/10.1016/j.nanoen.2022.107248
9 L.-L. Li, X.-D. Fan, K.-J. Wu, K. Sethanan, and M.-L. Tseng: Expert Syst. Appl. **237** (2023) 121406. https://doi.org/10.1016/j.eswa.2023.121406
10 M. Bouzerdoum, A. Mellit, and A. M. Pavan: Sol. Energy **98** (2013) 226. https://doi.org/10.1016/j.solener.2013.10.002

11 S. Theocharides, G. Makrides, A. Livera, M. Theristis, P. Kaimakis, and G. E. Georghiou: Appl. Energy **268** (2020) 115023. https://doi.org/10.1016/j.apenergy.2020.115023
12 H. Faris, M. A. Hassonah, A. M. Al-Zoubi, S. Mirjalili, and I. Aljarah: Neural Comput. Appl. **30** (2018) 2355. https://doi.org/10.1007/s00521-016-2818-2
13 H. Yu, Y. Chen, S. G. Hassan, and D. Li: Comput. Electron. Agric. **122** (2016) 94. https://doi.org/10.1016/j.compag.2016.01.019
14 A. Yona, T. Senjyu, T. Funabashi, and C.-H. Kim: IEEE Trans. Sustainable Energy **4** (2013) 527. https://doi.org/10.1109/TSTE.2013.2246591
15 J. Meng, M. Yue, and D. Diallo: IEEE Trans. Transp. Electrif. **9** (2022) 4898. https://doi.org/10.1109/TTE.2022.3209629
16 M. Seyedmahmoudian, E. Jamei, G. S. Thirunavukkarasu, T. K. Soon, M. Mortimer, B. Horan, A. Stojcevski, and S. Mekhilef: Energies **11** (2018) 1260. https://doi.org/10.3390/en11051260
17 N. Jaziri, J. Raymond, N. Giordano, and J. Molson: Energies **13** (2020) 96. https://doi.org/10.3390/en13010096